Title
Tuning Susceptibility via Misfit Strain in Relaxed Morphotropic Phase Boundary PbZr1-xTixO3 Epitaxial Thin Films

Journal
Advanced Materials Interfaces, 1(5)

ISSN
2196-7350

Authors
Agar, JC
Mangalam, RVK
Damodaran, AR
et al.

Publication Date
2014-08-01

DOI
10.1002/admi.201400098

Peer reviewed

ADVANCED MATERIALS INTERFACES
www.advmatinterfaces.de

Tuning Susceptibility via Misfit Strain in Relaxed Morphotropic Phase Boundary $PbZr_{1-x}Ti_xO_3$ Epitaxial Thin Films

*J. C. Agar, R. V. K. Mangalam, A. R. Damodaran, G. Velarde, J. Karthik, M. B. Okatan, Z. H. Chen, S. Jesse, N. Balke, S. V. Kalinin, and L. W. Martin**

Epitaxial strain is a powerful tool to manipulate the properties of ferroelectric materials. But despite extensive work in this regard, few studies have explored the effect of epitaxial strain on $PbZr_{0.52}Ti_{0.48}O_3$. Here we explore how epitaxial strain impacts the structure and properties of 75 nm thick films of the morphotropic phase boundary composition. Single-phase, fully epitaxial films are found to possess "relaxed" or nearly "relaxed" structures despite growth on a range of substrates. Subsequent studies of the dielectric and ferroelectric properties reveal films with low leakage currents facilitating the measurement of low-loss hysteresis loops down to measurement frequencies of 30 mHz and dielectric response at background dc bias fields as large as 850 kV/cm. Despite a seeming insensitivity of the crystal structure to the epitaxial strain, the polarization and switching characteristics are found to vary with substrate. The elastic constraint from the substrate produces residual strains that dramatically alter the electric-field response including quenching domain wall contributions to the dielectric permittivity and suppressing field-induced structural reorientation. These results demonstrate that substrate mediated epitaxial strain of $PbZr_{0.52}Ti_{0.48}O_3$ is more complex than in conventional ferroelectrics with discretely defined phases, yet can have a marked effect on the material and its responses.

1. Introduction

Ferroelectric materials have coupled mechanical, electrical, and thermal responses making them ideal for a wide variety of applications.[1–4] The $PbZr_{1-x}Ti_xO_3$ (PZT) family of ferroelectrics, for instance, possess large dielectric and piezoelectric responses, large polarization, low coercive fields, and high Curie temperatures.[5] The response of PZT can be tuned by applying chemical pressure (by varying Zr/Ti ratios) creating a competition between tetragonal (Ti-rich) and rhombohedral (Zr-rich) phases.[6] Between these phases exists a nearly temperature-independent boundary called the morphotropic phase boundary (MPB) (occurring at x = 0.48, henceforth referred to as MPB PZT).[7] Near this boundary, application of external stimuli can induce structural transitions giving rise to enhanced dielectric and piezoelectric susceptibility[7–9] which some have suggested arises as a result of a rotation of the polarization between variants.[10–12] Regardless, of the mechanism responsible for these effects, near-MPB compositions of PZT are commonly used in a variety of applications.[13–15]

Beyond chemical pressure, epitaxial thin-film strain has been extensively utilized to alter the response of ferroelectrics.[16] For instance, much work has been done on Ti-rich PZT variants and, in general, the lattice mismatch with the substrate acts via the Poisson relationship to exert a net change to the lattice structure that can induce changes in the magnitude of the spontaneous polarization, the transition temperature, and much more.[17–19] At a critical point, however, the material accommodates the growing strain energy by forming additional domain variants of the same phase but with a different orientation.[20,21] Considerably less work, however, has focused on using epitaxial strain to manipulate MPB PZT and, considering the relatively flat energy landscape near the MPB which eliminates the discrete nature of structural variants, the effects of such strain on the evolution of the structure and properties are expected to be less intuitive.[8,22,23] What little work that does exist in this regard, focuses on the structural evolution of relatively thick films (>200 nm)[24–26] with minimal emphasis on how the structure influences the properties.

Here we explore how epitaxial strain impacts the evolution of crystal and ferroelectric domain structure and the dielectric and ferroelectric properties of thin films of MPB PZT. 75 nm

J. C. Agar, Dr. R. V. K. Mangalam, A. R. Damodaran, G. Velarde, Dr. J. Karthik, Dr. Z. H. Chen, Prof. L. W. Martin
Department of Materials Science and Engineering and Materials Research Laboratory
University of Illinois
Urbana-Champaign
Urbana, IL 61801, USA,
E-mail: lwmartin@illinois.edu
Prof. L. W. Martin
Department of Materials Science and Engineering
University of California
Berkeley, Berkeley, CA 94720, USA
Dr. M. B. Okatan, Dr. S. Jesse, Dr. N. Balke, Dr. S. V. Kalinin
Center for Nanophase Materials Science
Oak Ridge National Laboratory
Oak Ridge, TN, USA

DOI: 10.1002/admi.201400098

thick, single-phase, fully epitaxial films of MPB PZT have been grown on a range of substrates that exhibit varying amounts of compressive lattice mismatch. Despite a broad range of strain conditions, X-ray diffraction studies show that all films possess "relaxed" or partially "relaxed" structures. Despite not exhibiting coherent epitaxial strain throughout the thickness of the film, the residual strain found in the MPB PZT films is found to greatly impact the evolution of properties in the material. Subsequent studies of the electronic, dielectric, and ferroelectric properties reveal films with low leakage currents capable of low-loss hysteresis loops down to measurement frequencies of 30 mHz and measurement of dielectric response at background dc bias fields as large as 850 kV/cm. Despite a practical insensitivity of the crystal structure to the lattice mismatch and strain, the saturation polarization and switching characteristics are found to vary systematically with the underlying substrate. Both local-probes and macroscopic capacitor-based studies suggest that the elastic boundary conditions from the various substrates produce residual strain which varies inversely with lattice mismatch and can dramatically alter the electric-field response. In particular, the elastic constraints can quench domain wall contributions to the dielectric permittivity and suppress field-induced structural reorientation along the field direction. Overall, these results demonstrate that epitaxial strain control of MPB PZT is more complex than in conventional ferroelectrics with discretely defined phases, but control of the lattice mismatch can have a marked effect on the material and its responses.

2. Results and Discussion

75 nm $PbZr_{0.52}Ti_{0.48}O_3$/25 nm $SrRuO_3$/$SrTiO_3$ (001) (a = 3.905 Å), $DyScO_3$ (110) (pseudocubic a_{pc} = 3.944 Å), and $NdScO_3$ (110) (pseudocubic a_{pc} = 4.013 Å) heterostructures were grown via pulsed-laser deposition (PLD) (see Experimental Section). The compressive lattice mismatch between the tetragonal- (rhombohedral-) versions of MPB PZT and $SrTiO_3$, $DyScO_3$, and $NdScO_3$ are 3.58% (4.05%), 2.62% (3.10%), and 0.91% (1.40%), respectively. Atomic force microscopy (AFM) images reveal smooth, atomically terraced surfaces with root-mean-square surface roughness of <0.5 nm (**Figure 1**a). Domain structures were probed using vertical band-excitation piezoresponse force microscopy (BE-PFM) (see Experimental Section) and a typical BE-PFM amplitude image for all heterostructures is displayed (Figure 1b–d).[27] There are very few published PFM images of the domain structure of epitaxial MPB PZT and the application of BE-PFM imaging provides potentially the best opportunity to image this fine-scale and highly-susceptible domain structure. From our imaging, all films exhibit similar mosaic domain structures with features on the order of 25–200 nm and it is possible that we are not able to resolve smaller-scale nanodomains that have been observed in transmission electron microscopy studies.[28,29] In turn, although the BE-PFM images provide some indication of disorder and the nature of the domain structure at a length scale >20 nm, it does not provide an exact visual representation of the differences between the films. We also note that there was no observed phase contrast in these images, consistent with films that are fully downward poled due to the presence of the bottom electrode.

To gather additional insight into the differences, the samples were probed by X-ray diffraction. All heterostructures were revealed to be fully 00*l*-oriented, single-phase films with no evidence of secondary phases (**Figure 2**a). Subsequent asymmetric X-Ray diffraction reciprocal space mapping (RSM) studies about the 103-diffraction condition of the MPB PZT (Figure 2b–d) indicate that the MPB PZT films possess considerably broadened diffraction peaks (with smearing towards the cubic line) and, regardless of substrate, a nearly relaxed structure. We note that the broadened diffraction peaks makes accurate determination of the lattice parameter and phase distribution difficult and that the observed broadening is likely the consequence of a number of features. First, it is known that anomalous diffraction caused by coherent scattering from nanotwinned domains[30,31] can result in broaden diffraction peaks. Second, the presence of inhomogeous strain in the films could also give rise to broaden diffraction peaks. Close inspection reveals slight differences between the films where as the misfit strain decreases (i.e., moving from $SrTiO_3$ to $NdScO_3$) the diffraction peak is observed to broaden towards larger Q_x-values (commensurate with increased substrate coherency) while the Qy-values remain relatively unchanged between the films. This subtle change in the diffraction peak shape suggests that even though the films are not perfectly, coherently strained, some level of residual strain from the lattice mismatch is found to persist in the films with the lowest lattice mismatch. This is a bit surprising, but potentially explained by the fact that large lattice mismatches can be readily accommodated by film relaxation via structural variation, domain formation, etc. in the films on $SrTiO_3$ and $DyScO_3$ and only the films on $NdScO_3$ exhibit a small amount of unrelaxed strain. In the latter case, the compressive lattice mismatch effectively

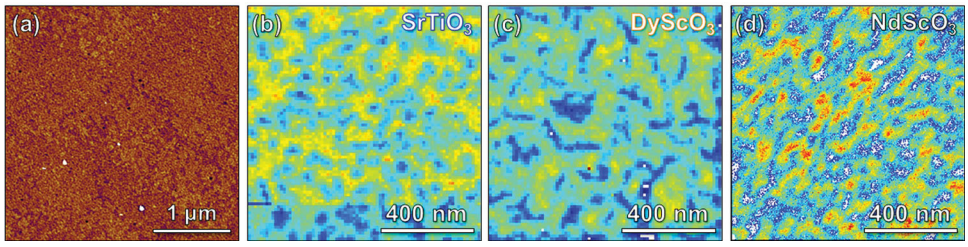

Figure 1. a) Atomic force microscopy topography image of a typical 75 nm $PbZr_{0.52}Ti_{0.48}O_3$/25 nm $SrRuO_3$/$SrTiO_3$ (001) heterostructure. Representative vertical band excitation piezoresponse force microscopy amplitude images of 75 nm $PbZr_{0.52}Ti_{0.48}O_3$/25 nm $SrRuO_3$ heterostructures grown on b) $SrTiO_3$ (001), c) $DyScO_3$ (110), and d) $NdScO_3$ (110) substrates.

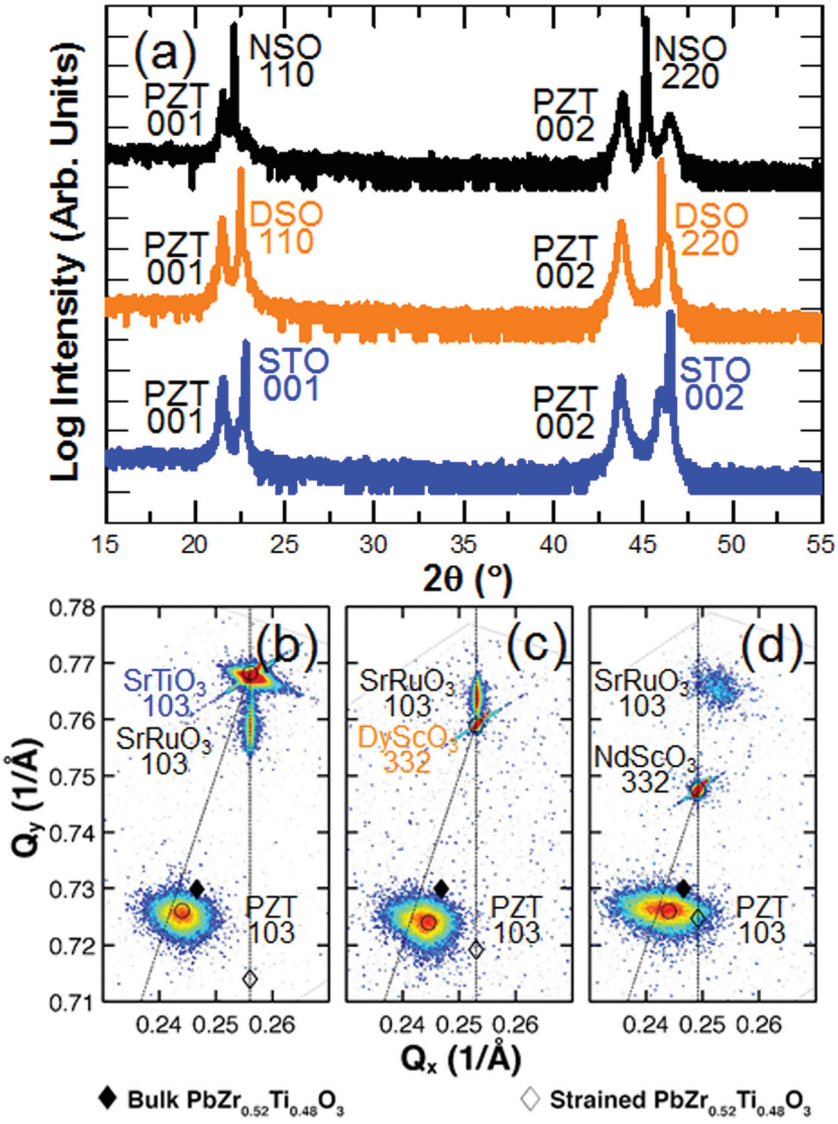

Figure 2. a) θ-2θ X-ray diffraction pattern about the 002-diffraction condition for 75 nm $PbZr_{0.52}Ti_{0.48}O_3$/25 nm $SrRuO_3$ heterostructures grown on $SrTiO_3$ (001), $DyScO_3$ (110), and $NdScO_3$ (110) substrates (bottom-to-top of graph). Asymmetric reciprocal-space mapping studies about the 103- and 332-diffraction condition for heterostructures grown on b) $SrTiO_3$ (001), c) $DyScO_3$ (110), and d) $NdScO_3$ (110) substrates. Substrate and film peak location marked by the circular marker. The bulk (solid) and strained (open) $PbZr_{0.52}Ti_{0.48}O_3$ tetragonal peak is indicated with a diamond.

drives the structure towards slightly increased tetragonality. These observations differ dramatically from similar studies of, for instance, $PbZr_{0.2}Ti_{0.8}O_3$ where changing the substrate (even in thicker films) results in coherently strained out-of-plane oriented *c* domains that are punctuated by varying densities of in-plane oriented *a* domains to accommodate the overall strain state.[32] For MPB PZT, however, even in only 75 nm thick films the presence of a number of structural degrees of freedom appears to result in rapid accommodation of the strain and the inability to apply epitaxial strains in the same regard. Thus, in the end, only films with small lattice mismatches exhibit any strain effects, and all others are fully relaxed. Similar effects on the structure of MPB PZT films have been observed in studies of microfabricated films where the production of micro-scale features can locally release the in-plane strain of the film.[24]

Even though the structural and domain characterization suggests minimal differences between the heterostructures, subsequent studies of the electrical, dielectric, and ferroelectric properties reveal intriguing differences. These studies were conducted at room temperature using circular capacitor structures (25–100 μm in diameter) with symmetric $SrRuO_3$ electrodes.[33] Leakage measurements show highly symmetric response with low currents (implying minimal electrode induced imprint in the films) (**Figure 3**a) and comparison with similarly processed 150 nm $PbZr_{0.2}Ti_{0.8}O_3$ heterostructures reveal that the MPB PZT films exhibit orders-of-magnitude lower leakage currents as expected.[34] Overall, the high quality of these films is evident and enables non-traditional studies of ultra-slow ferroelectric hysteresis loops and dielectric measurements at high bias fields.

The ferroelectric properties of the various MPB PZT heterostructures were probed as a function of frequency between 0.03–20,000 Hz and underwent ferroelectric switching without significant losses even at the lowest frequencies. Characteristic hysteresis loops for all heterostructures measured at 1 kHz are provided (Figure 3b). All loops are well-saturated, with P_S ~ 35–38 μC/cm^2 which increases (slightly) with decreasing lattice mismatch between film and substrate – consistent with the structural studies which suggest a similar trend in increasing residual strain. A similar trend persists in the horizontal offset of the hysteresis loops which increases from 6.5 kV/cm to 18.5 kV/cm for heterostructures grown on $SrTiO_3$ and $NdScO_3$ substrates, respectively, and is indicative of strain gradients from the residual strain.[35–37]

Frequency-dependent ferroelectric hysteresis loop studies, spanning eight decades of frequency, were completed and representative data for heterostructures grown on $SrTiO_3$ substrates are provided (Figure 3c) (see Supporting Information for data for all heterostructures, Figure S1). These studies reveal the presence of features which can potentially be related to a field-induced structural transition. As the frequency of measurement was decreased there is evidence of a transition near ~150 kV/cm resulting in a change in slope of the hysteresis loop (inset, Figure 3c). This transition is not observed in the films with increased residual strain (i.e., those on $DyScO_3$ to $NdScO_3$) where the strain acts to promote increased tetragonality.

The role of this residual strain can be visualized by probing the differences in switched area during local switching in

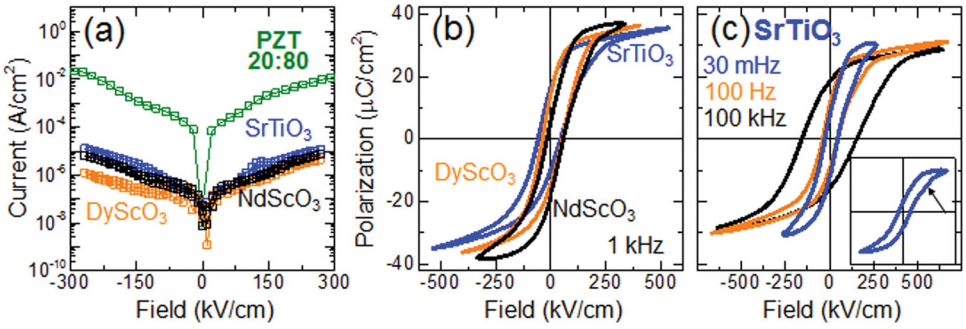

Figure 3. Electrical measurement of 75 nm $PbZr_{0.52}Ti_{0.48}O_3$ / 25 nm $SrRuO_3$ on various substrates. a) Current-voltage measurements (including, for comparison, 100 nm $PbZr_{0.2}Ti_{0.8}O_3$/25 nm $SrRuO_3$/$GdScO_3$ (110) heterostructure). b) Ferroelectric hysteresis loops measured at 1 kHz. c) Ferroelectric hysteresis loops for a $PbZr_{0.52}Ti_{0.48}O_3$/$SrRuO_3$/$SrTiO_3$ (001) heterostructure taken at various frequencies. The inset shows the transition region observed in ferroelectric hysteresis loops at 30 mHz, indicated by the black arrow. All hysteresis loops are composed of a minimum of 150 data points.

the different heterostructures. 100 points, within a pre-poled region, were switched in a 10 × 10 array and at each point PFM phase loops indicated that the film underwent ferroelectric switching to saturation (see Experimental section and Supporting Information, Figure S2). Amplitude images from BE-PFM imaging following the switching studies on heterostructures grown on $SrTiO_3$ (**Figure 4**a) and $NdScO_3$ (Figure 4b) reveal that the heterostructures grown on $SrTiO_3$ have a significantly larger switched area keeping all other factors constant (i.e., switching waveform, PFM tip, contact set-point, etc.). There was no appreciable difference in the observed switched area for the heterostructures grown on $DyScO_3$ and $NdScO_3$ (see Supporting Information, Figure S2). The switched area was extracted by counting the number of pixels which exhibit phase inversion from the pre-poled state (see Supporting Information, Figure S2) and a histogram of this data confirms the visual observations (Figure 4c). The reduced switched area observed in films with increased residual strain (i.e., $DyScO_3$ to $NdScO_3$) could be the result of elastic constraints from the substrate that promote back switching following a switching pulse due to the built-in potential in the film. In the end, the presence of an elastic constraint (in the form of a residual epitaxial strain) dramatically impacts the nature of switching and, in general, the electric-field dependence of the films.

The data thus far have illustrated how the elastic constraints from the residual epitaxial strain can impact the field-induced structural evolution, in turn, impacting switching in the material. Here we move on to probe the implications of the residual strain on the low-field response – in particular the dielectric permittivity with a special focus on how these elastic constraints impact domain wall contributions. We have completed two measurements: 1) Rayleigh studies with increasing ac excitation field and 2) frequency-dependent permittivity measurements at increasing background dc bias to extract the domain wall contributions to the permittivity. For the Rayleigh studies we report both the dielectric permittivity (**Figure 5**a) and loss tangent (Figure 5b) as a function of increasing ac excitation bias. Reversible domain wall contributions are found to persist up to ~1.33 kV/cm and below this point the dielectric permittivity of all heterostructures is similar (611–640) and at the low end of previously published values for MPB PZT films (values vary from 600–1300 depending on thickness, processing, and preferred orientation for polycrystalline films)[9,38,39] and are likely the result of the elastic constraint of the substrate which suppresses domain wall and structural contributions.[40–42] Corresponding frequency dependent studies of the dielectric permittivity and loss tangent (using an excitation bias of 1 kV/cm, within the reversible regime) have been completed (Figure 5c,d). It is worth noting that the dielectric loss increases drastically upon increasing the measurement frequency above 1–10 kHz; a feature not observed in thin films of non-MPB PZT synthesized and probed in a similar fashion. We correlate this to the potential freezing out of sluggish domain wall contributions or collective responses to the dielectric response in MPB PZT.[43,44] The loss tangent is also found to increase in the frequency regime where the feature observed in the hysteresis loops, which we attribute to a possible structural phase transition near ~150 kV/cm (Figure 3c), is no longer observed in the measurments.

Returning now to focus on the ac field dependent Rayleigh studies, within the Rayleigh regime (demarcated by the dashed lines, Figure 5a) the ac field dependence of the permittivity was fitted to the Rayleigh law $\varepsilon_r = \varepsilon_{init} + \alpha E_0$ ($r^2 > 0.98$) where ε_r is the permittivity, E_0 is the amplitude of the electric field, and ε_{init} and α are the reversible and irreversible domain wall contributions

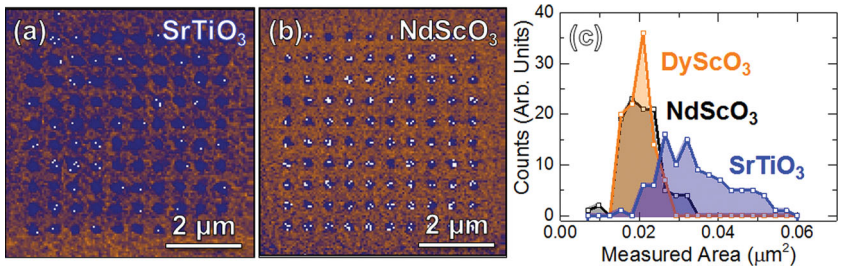

Figure 4. Band excitation piezoresponse force microscopy amplitude images following single point band excitation piezoresponse force switching studies for 75 nm $PbZr_{0.52}Ti_{0.48}O_3$/25 nm $SrRuO_3$ heterostructures grown on a) $SrTiO_3$ (001) and b) $NdScO_3$ (110) substrates. c) The average switched area extracted from the band excitation piezoresponse force phase image is represented in a histogram – indicating on average larger switched domains in heterostructurs on $SrTiO_3$ as compared to the heterostructures on $DyScO_3$ and $NdScO_3$ substrates.

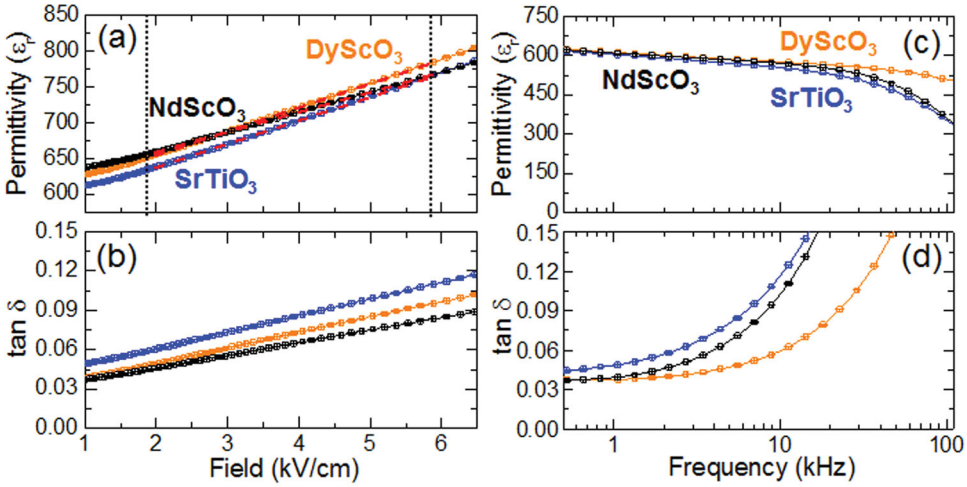

(e)

	ε_{init}	α (cm/kV)
$SrTiO_3$	573.1 ± 0.3	33.4 ± 0.1
$DyScO_3$	588 ± 0.2	33.3 ± 0.08
$NdScO_3$	603 ± 0.1	29.9 ± 0.03

Figure 5. a) Dielectric permittivity and b) loss tangent for all heterostructure variants displayed as a function of ac excitation bias represented as field. Frequency dependence of the c) dielectric permittivity and d) loss tangent for all heterostructure variants. e) Fits to the Rayleigh regime (marked by the black dashed lines and red linear fits in a) reveal values of for ε_{init} and α.

to the dielectric permittivity, respectively (Figure 5e).[45,46] Here we focus on the α values (29.9–33.4 cm/kV) which are an order of magnitude larger than values extracted from $PbZr_{0.2}Ti_{0.8}O_3$ (1.4 cm/kV) and $PbZr_{0.8}Ti_{0.2}O_3$ (2.08 cm/kV) heterostructures prepared in a similar fashion,[37] significantly lower than those reported for bulk MPB samples, and comparable to values reported for polycrystalline MPB films.[47,48] Although the range observed for our heterostructures is somewhat narrow, the films possessing the most residual strain (i.e., those grown on $NdScO_3$ substrates) are found to possess a reduced α value suggesting that the elastic constraints impact the domain wall contributions to response in these materials.

The Rayleigh studies are further supported by applied background dc electric field studies (see Experimental Section) which can suppress the extrinsic (domain wall) contributions allowing for a quantitative measure of the intrinsic response.[49] This is achieved by fitting the frequency dependence (from 1–100 kHz) of the permittivity at each applied background dc electric field (from 0 to –850 kV/cm) to the equation $\varepsilon = \varepsilon_i - \alpha \log f$ and extracting the field-dependence of the intercept (ε_i) and slope (α). Using this approach, the field at which extrinsic contributions are suppressed and the zero-field intrinsic permittivity of a material can be extracted. Such background dc electric field measurements have been applied to the various MPB PZT heterostructures as well as similarly prepared 100 nm $PbZr_{0.2}Ti_{0.8}O_3$ and $PbZr_{0.8}Ti_{0.2}O_3$ heterostructures. A typical dataset from such studies is provided for the case of a MPB PZT heterostructure grown on $SrTiO_3$ (**Figure 6**a) (see Supporting Information for data for all heterostructures, Figure S3). The permittivity and slope of the frequency response decrease as the background dc bias field increases as a result of freezing out the extrinsic contributions to response at high fields.[50,51] We then plot the field-dependence of the intercept (ε_i) as a function of the background dc electric field for all heterostructure variants (Figure 6b-f). These plots show two regimes, a low-field regime (where the response consists of both intrinsic and extrinsic contributions, shown in green) and a high-field regime (where the response is thought to be reflective of only the intrinsic response, shown in purple). The slope and intercepts of linear fits in the low-field regime correspond to the extrinsic tunability (α_e, which describes how the applied dc electric field suppresses the extrinsic response) and the zero-field permittivity (ε_e), respectively. The slope and intercepts of linear fits in the high-field regime correspond to the intrinsic tunability (α_i, which describes how the external dc electric field suppresses the intrinsic response) and the zero-field intrinsic permittivity (ε_i), respectively.

In the low-field regime the MPB PZT films have nearly identical ε_e (625–700) which are considerably larger than those for $PbZr_{0.2}Ti_{0.8}O_3$ (272) and somewhat larger than that for $PbZr_{0.8}Ti_{0.2}O_3$ (549). Furthermore, the α_e values of the MPB PZT heterostructures are similar indicating that the field-dependence of the extrinsic contributions are comparable (–2.65 to –3.06 cm/kV) and similar to that for $PbZr_{0.8}Ti_{0.2}O_3$ (–3.04 cm/kV), but much larger than that for $PbZr_{0.2}Ti_{0.8}O_3$ (–0.36 cm/kV). Upon application of higher fields, we again see a difference between the MPB PZT (and $PbZr_{0.8}Ti_{0.2}O_3$) heterostructures which undergo the transition to the high-field regime (where extrinsic contributions are quenched) at fields of magnitude 100–200 kV/cm and the $PbZr_{0.2}Ti_{0.8}O_3$ heterostructures which do not transition until fields of magnitude 400 kV/cm. Finally, in the high-field regime, MPB PZT and $PbZr_{0.8}Ti_{0.2}O_3$ heterostructures exhibit comparable α_i (–0.07 to –0.11 cm/kV) and ε_i (163–179) while the $PbZr_{0.2}Ti_{0.8}O_3$ heterostructures have

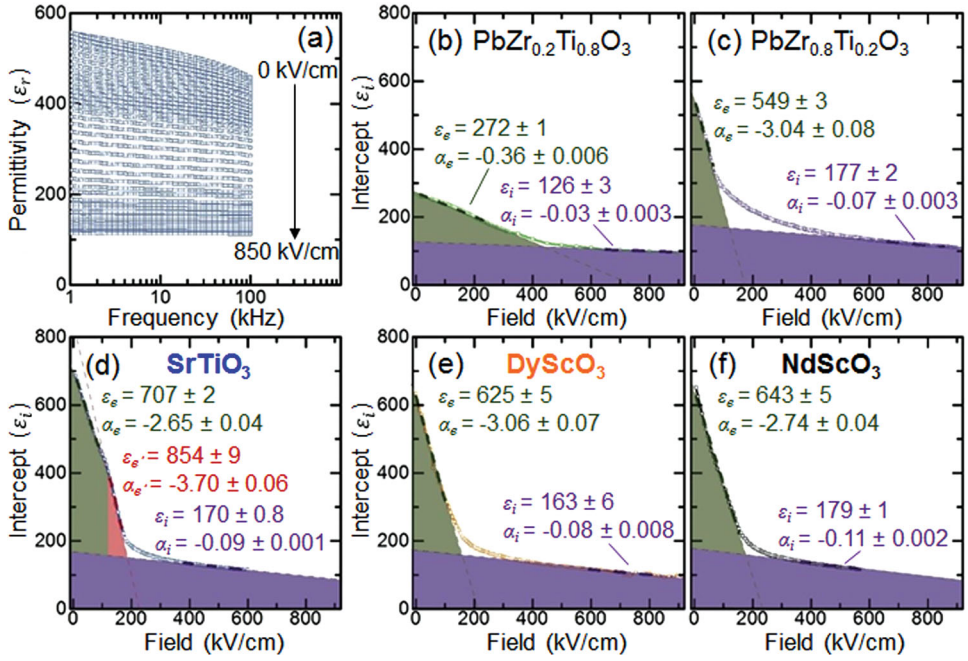

Figure 6. a) Typical dielectric permittivity as a function of frequency measured at increasing background fields for a 75 nm $PbZr_{0.52}Ti_{0.48}O_3$/25 nm $SrRuO_3$/$SrTiO_3$ (001) heterostructure. Extracted zero frequency permittivity as a function of increasing background fields for b) $PbZr_{0.2}Ti_{0.8}O_3$, c) $PbZr_{0.8}Ti_{0.2}O_3$, and $PbZr_{0.52}Ti_{0.48}O_3$ heterostructures grown on (d) $SrTiO_3$ (001), e) $DyScO_3$ (110), and f) $GdScO_3$ (110) substrates. Regions where linear fits were computed are represented by the purple, red, and green dashed lines for the intrinsic, intermediate, and extrinsic regimes, respectively.

reduced α_i (–0.03 cm/kV) and ε_i (126) (consistent with prior reports).[49,52]

There are a number of features worth highlighting from this analysis. Overall the MPB PZT and $PbZr_{0.8}Ti_{0.2}O_3$ heterostructures show markedly different response from the $PbZr_{0.2}Ti_{0.8}O_3$ heterostructures which can be understood in the context of their domain structures and elastic coupling with the substrate. First, ε_i increases as we move to compositions possessing more Zr. This can be readily understood by the fact that as the Zr-content increases the excitation field is applied increasingly along non-polar directions exciting additional intrinsic contributions to the permittivity. Second, α_i values are the largest in the MPB PZT heterostructures, intermediate for the $PbZr_{0.8}Ti_{0.2}O_3$, and smallest for $PbZr_{0.2}Ti_{0.8}O_3$ suggesting that the intrinsic instabilities of the MPB PZT provide for additional tunability. Third, ε_e is larger for both the MPB PZT and $PbZr_{0.8}Ti_{0.2}O_3$ than for $PbZr_{0.2}Ti_{0.8}O_3$ likely due to the higher density of domain walls which gives rise to a greatly enhanced extrinsic contribution to the permittivity. Finally, the α_e values for MPB PZT and $PbZr_{0.8}Ti_{0.2}O_3$ are similar and nearly an order of magnitude larger than that of $PbZr_{0.2}Ti_{0.8}O_3$ which is likely the result of a combination of effects including the adaptability of the domain structure and the elastic interactions within the film and between the film and substrate. In these measurements we pole the sample and then measure with increasing fields applied along that same direction which quenches or minimizes domain wall contributions from ferroelectric (i.e., 180°) domain walls and limits the response to ferroelastic (i.e., non-180°) domain walls. The large α_e for the MPB PZT heterostructures results from the adaptive nature of the structure and the nearly flat energy landscape in this material which allows for large susceptibility. Additionally, because of this adaptability the system can readily adjust the volume surrounding an excited area to accommodate the additional strain energy that forms, thereby reducing the clamping effect of the film and substrate (as evidenced by the insensitivity of the material to the changing lattice mismatch from the substrates). On the other hand, in $PbZr_{0.2}Ti_{0.8}O_3$, the domain structure that forms (i.e., *c*/*a*/*c*/*a*) is the result of the elastic boundary conditions of the substrate and thus it is extraordinarily difficult to adjust the domain structure as the domains are strongly coupled to the total strain state of the film. In turn, not only does this reduce the extrinsic tunability, but it also increases the critical field required to suppress the stiffened domain wall contributions.

The final feature to highlight is found in the MPB PZT heterostructures grown on $SrTiO_3$ substrates. A regime of enhanced susceptibility (occurring between 100–200 kV/cm) is observed (red area, Figure 5d) in which there is a change in the slope of the extrinsic tunability. This regime matches the location of the feature observed in the ferroelectric hysteresis loops (Figure 3c). Within this region of enhanced susceptibility α_e ~ 850 and ε_e ~ –3.7 cm/kV, which are both considerably larger than observed in all other low-field regimes for all samples. It is possible that this enhanced response arises in the MPB PZT samples possessing the least residual strain as a result of the a field induced structural transformation towards the applied electric field direction. Such a structural transition could potentially be suppressed in heterostructures grown on substrates with smaller lattice mismatch that possess larger amounts of residual strain (i.e., $DyScO_3$ to $NdScO_3$).

3. Conclusions

Overall this manuscript takes an in-depth look at how epitaxial strain in the form of lattice mismatch can impact the evolution of crystal and domain structure and ultimately the properties of MPB PZT. In general, this work highlights the complexity of strain evolution in the highly-adaptable MPB PZT material and how the innate flat energy landscape can skirt classical assumptions of epitaxial thin-film strain. In the end, high-quality, single-phase films of MPB PZT were shown to exhibit significantly different field induced dielectric permittivity when grown on various substrates despite the appearance of "relaxed" crystal structure. Local probes of switching in these heterostructures reveal distinct differences in the average switched area of the heterostructures depending on the lattice mismatch with the substrate and therefore the corresponding elastic boundary conditions. Subsequent dielectric and ferroelectric studies reveal transitions in ferroelectric switching at ultra-low frequencies and in the dielectric response at high dc fields that suggest that reduced residual strain promotes full adaptability of the structure under applied fields and, as a result, enhanced electric field susceptibility. Overall, MPB PZT – and other systems with highly-adaptable structures – may not be beholden to the classic effects of epitaxial strain in the same manner as more conventional materials. Nonetheless, the role of strain or residual strains in materials possessing elastic order is something that must not be overlooked and can lead to non-intuitive observations.

4. Experimental Section

Film Growth: 75 nm thick $PbZr_{0.52}Ti_{0.48}O_3$/25 nm $SrRuO_3$/$SrTiO_3$ (001), $DyScO_3$ (110), and $NdScO_3$ (110) heterostructures were grown via pulsed-laser deposition in an on-axis geometry (target-to-substrate spacing of 6.3 cm). The $SrRuO_3$ was deposited from a stoichiometric target at 645 °C in a 100 mTorr pressure of oxygen at a laser fluence of 1.2 J cm^{-2} at a laser frequency of 14 Hz. The $PbZr_{0.52}Ti_{0.48}O_3$ was deposited from a $Pb_{1.1}Zr_{0.52}Ti_{0.48}O_3$ target at 625 °C in a 200 mTorr pressure of oxygen at a laser fluence of 1.3 J cm^{-2} at a laser frequency of 2 Hz. Following growth samples were cooled in 700 mTorr of oxygen at a rate of 5 °C/min.

Band Excitation Piezoresponse Force Microscopy (BE-PFM) and Switching Studies: BE-PFM was conducted on a modified Asylum Research Cypher Atomic Force Microscope at Oak Ridge National Laboratory. Images were acquired using a chirp waveform of 1 V amplitude with a bandwidth of 60 kHz near the tip resonance frequency. At each point the band excitation signal was repeated 4 times as a means of averaging the response. Following measurement the cantilever response was fitted to a simple harmonic oscillator (SHO) model at each point, allowing the extraction of amplitude, phase, cantilever resonance frequency, and quality factor. Studies of the switched area were completed in a 10 × 10 grid within a 5 × 5 μm region in the center of a 6.5 × 6.5 μm region that was previously poled at 10 V. At each point ferroelectric switching was achieved twice using two 64-step, 9 V triangular waveforms. Following the BE-SS, BE-PFM images were taken where the vertical axis is the slow scan direction. The switched area was determined by counting the number of pixels with 180° phase inversion at each of the switched points using MATLAB image processing toolbox.

Dielectric and Ferroelectric Measurements: All electrical measurements were conducted in a dark, vibration and noise isolated chamber with the drive bias being applied to the top electrode. Dielectric permittivity was calculated from the capacitance (C) using $C=\frac{\varepsilon_r \varepsilon_0 A}{d}$ where A is the area of the capacitor, d is the thickness of the film, and ε_0 is the permittivity of free space. Prior to dielectric measurement all samples were switched >50 times, left poled in the negative direction, and allowed to equilibrate for 2 minutes prior to measurement. All Rayleigh (ac excitation-dependent) studies were conducted at 1 kHz and all frequency-dependent studies were completed at an ac excitation amplitude of 8 mV (rms). The background dc bias studies were all taken with negative applied dc bias and an ac excitation amplitude of 8 mV (rms). Prior to the background dc bias experiments, the capacitors were poled with a 1 second –5 V pulse and allowed to equilibrate for 2 minutes. Similarly at each voltage step the capacitor was allowed to equilibrate for 30 seconds prior to measurement. Linear fits of the capacitance frequency curves at increasing dc bias was taken excluding regions where the dielectric loss exceeded 0.15.

Supporting Information

Supporting Information is available from the Wiley Online Library or from the author.

Acknowledgements

J. C. A. and L. W. M. would like to acknowledge support from the National Science Foundation under grant DMR-1149062 and the Air Force Office of Scientific Research (AFOSR) under grant AF FA 9550–11–1–0073. R.V.K.M. and L.W.M. would like to acknowledge support from the National Science Foundation under grant DMR-1124696. A.R.D. and L.W.M. would like to acknowledge support from the Army Research Office (ARO) under grant W911NF-10–1–0482. J.K. and L.W.M. would like to acknowledge support from the Office of Naval Research (ONR) under grant N00014–10–1–0525.

Received: February 21, 2014
Revised: April 6, 2014
Published online: May 15, 2014

[1] S. H. Baek, J. Park, D. M. Kim, V. A. Aksyuk, R. R. Das, S. D. Bu, D. A. Felker, J. Lettieri, V. Vaithyanathan, S. S. N. Bharadwaja, N. Bassiri-Gharb, Y. B. Chen, H. P. Sun, C. M. Folkman, H. W. Jang, D. J. Kreft, S. K. Streiffer, R. Ramesh, X. Q. Pan, S. Trolier-McKinstry, D. G. Schlom, M. S. Rzchowski, R. H. Blick, C. B. Eom, *Science.* **2011**, *334,* 958–961.
[2] M. Dawber, K. M. Rabe, J. F. Scott, *Rev. Mod. Phys.* **2005**, *77*, 1083–1130.
[3] N. Setter, D. Damjanovic, L. Eng, G. Fox, S. Gevorgian, S. Hong, A. Kingon, H. Kohlstedt, N. Y. Park, G. B. Stephenson, I. Stolitchnov, A. K. Taganstev, D. V. Taylor, T. Yamada, S. Streiffer, *J. Appl. Phys.* **2006**, *100*(5), 051606.
[4] J. F. Scott, *Science.* **2007**, *315*, 954–959.
[5] N. Izyumskaya, Y. Alivov, S. Cho, H. Morkoç, H. Lee, Y. Kang, *Crit. Rev. Solid State Mater. Sci.* **2007**, *32*, 111–202.
[6] P. Gerber, U. Bottger, R. Waser, *J. Appl. Phys.* **2006**, *100,* 124105.
[7] B. Jaffe, R. S. Roth, S. Marzullo, *J. Appl. Phys.* **1954**, *25*, 809–810.
[8] D. Damjanovic, *Appl. Phys. Lett.* **2010**, *97*, 062906.
[9] T. Oikawa, M. Aratani, H. Funakubo, K. Saito, M. Mizuhira, *J. Appl. Phys.* **2004**, *95*, 3111–3115.
[10] B. Noheda, J. A. Gonzalo, L. E. Cross, R. Guo, S. Park, D. E. Cox, G. Shirane, *Phys. Rev. B.* **2000**, *61*, 8687–8695.
[11] H. Fu, R. E. Cohen, *Nature* **2000**, *403*, 281.
[12] L. Bellaiche, A. García, D. Vanderbilt, *Phys. Rev. B.* **2001**, *64*, 060103.

[13] S. Park, T. R. Shrout, *IEEE Trans. Ultrason. Ferroelectrics Freq. Cont.* **1997**, *44*, 1140–1147.
[14] N. Ledermann, P. Muralt, J. Baborowski, S. Gentil, K. Mukati, M. Cantoni, A. Seifert, N. Setter, *Sens. Actu. A.* **2003**, *105*, 162–170.
[15] R. Chukka, J. W. Cheah, Z. Chen, P. Yang, S. Shannigrahi, J. Wang, L. Chen, *Appl. Phys. Lett.* **2011**, *98*, 242902–242903.
[16] D. G. Schlom, L. Chen, C. Eom, K. M. Rabe, S. K. Streiffer, J. Triscone, *Ann. Rev. Mater. Res.* **2007**, *37*, 589–626.
[17] J. Karthik, A. R. Damodaran, L. W. Martin, *Phys. Rev. Lett.* **2012**, *108*, 167601.
[18] I. Vrejoiu, G. Le Rhun, L. Pintilie, D. Hesse, M. Alexe, U. Gösele, *Adv Mater.* **2006**, *18*, 1657–1661.
[19] V. Nagarajan, I. G. Jenkins, S. P. Alpay, H. Li, S. Aggarwal, L. Salamanca-Riba, A. L. Roytburd, R. Ramesh, *J. Appl. Phys.* **1999**, *86*, 595–602.
[20] J. Karthik, L. W. Martin, *Phys. Rev. B.* **2011**, *84*, 024102.
[21] N. A. Pertsev, A. G. Zembilgotov, A. K. Tagantsev, *Phys. Rev. Lett.* **1998**, *80*, 1988–1991.
[22] J. Ouyang, W. Zhang, S. P. Alpay, A. Roytburd, *J. Adv. Ceram.* **2013**, *2*, 1–10.
[23] W. Liu, X. Ren, *Phys. Rev. Lett.* **2009**, *103*, 257602.
[24] K. Lee, S. Baik, *Appl. Phys. Lett.* **2005**, *86*, 202901.
[25] S. Yokoyama, H. Funakubo, H. Morioka, K. Saito, T. Yamada, M. Ishikawa, *Ferroelectrics.* **2009**, *389*, 10–17.
[26] S. Yokoyama, H. Morioka, Y. K. Kim, H. Nakaki, H. Funakubo, K. Saito, K. Nishida, T. Katoda, *J. Mater. Res.* **2007**, *22*, 1551–1557.
[27] S. Jesse, S. V. Kalinin, *J. Phys. D.* **2011**, *44*, 464006.
[28] L. A. Schmitt, K. A. Schönau, R. Theissmann, H. Fuess, H. Kungl, M. J. Hoffmann, *J. Appl. Phys.* **2007**, *101*, 074107.
[29] F. Xu, S. Trolier-McKinstry, W. Ren, B. Xu, Z. Xie, K. J. Hemker, *J. Appl. Phys.* **2001**, *89*, 1336–1348.
[30] Y. U. Wang, *Phys. Rev. B.* **2006**, *74*, 104109.
[31] R. Theissmann, L. A. Schmitt, J. Kling, R. Schierholz, K. A. Schonau, H. Fuess, M. Knapp, H. Kungl, M. J. Hoffmann, *J. Appl. Phys.* **2007**, *102*, 024111.
[32] J. Karthik, A. R. Damodaran, L. W. Martin, *Phys. Rev. Lett.* **2012**, *108*, 167601.
[33] J. Karthik, A. R. Damodaran, L. W. Martin, *Adv. Mater.* **2012**, *24*, 1610–1615.
[34] Z. Wróbel, *Phys. Stat. Solidi (a)*. **1978**, *45*, K67–K69.
[35] M. Brazier, M. McElfresh, S. Mansour, *Appl. Phys. Lett.* **1999**, *74*, 299–301.
[36] D. Lee, A. Yoon, S. Y. Jang, J. Yoon, J. Chung, M. Kim, J. F. Scott, T. W. Noh, *Phys. Rev. Lett.* **2011**, *107*, 057602.
[37] R. V. K. Mangalam, J. Karthik, A. R. Damodaran, J. C. Agar, L. W. Martin, *Adv. Mater.* **2013**, *25*, 1761–1767.
[38] D. A. Berlincourt, C. Cmolik, H. Jaffe, *Proc. Inst. Radio Eng.* **1960**, *48*, 220–229.
[39] Y. Bastani, N. Bassiri-Gharb, *Acta Mater.* **2012**, *60*, 1346–1352.
[40] C. Zhou, D. M. Newns, *J. Appl. Phys.* **1997**, *82*, 3081–3088.
[41] M. E. Drougard, R. Landauer, *J. Appl. Phys.* **1959**, *30*, 1663–1668.
[42] N. Bassiri-Gharb, I. Fujii, E. Hong, S. Trolier-McKinstry, D. Taylor, D. Damjanovic, *J. Electroceram.* **2007**, *19*, 49–67.
[43] J. O. Gentner, P. Gerthsen, N. A. Schmidt, R. E. Send, *J. Appl. Phys.* **1978**, *49*, 4485–4489.
[44] U. Robels, G. Arlt, *J. Appl. Phys.* **1993**, *73*, 3454–3460.
[45] D. Damjanovic, D. V. Taylor, *Ferroelectrics.* **1999**, *221*, 137–146.
[46] D. V. Taylor, D. Damjanovic, *J. Appl. Phys.* **1997**, *82*, 1973–1975.
[47] R. E. Eitel, T. R. Shrout, C. A. Randall, *J. Appl. Phys.* **2006**, *99*, 124110.
[48] F. Griggio, S. Jesse, A. Kumar, O. Ovchinnikov, H. Kim, T. N. Jackson, D. Damjanovic, S. V. Kalinin, S. Trolier-McKinstry, *Phys. Rev. Lett.* **2012**, *108*, 157604.
[49] M. Narayanan, S. Tong, S. Liu, B. Ma, U. Balachandran, *Appl. Phys. Lett.* **2013**, *102*, 062906.
[50] D. Damjanovic, *Rep. Prog. Phys.* **1998**, *61*, 1267.
[51] J. M. Herbert, *Ferroelectric Transducers and Sensors*, 3rd Ed., (Ed. D. S. Campbell), Gordon and Breach Science Publishers **1982**.
[52] R. V. K. Mangalam, J. C. Agar, A. R. Damodaran, J. Karthik, L. W. Martin, *ACS Appl. Mater. Interfaces.* **2013**, *24*, 13235–13241.